Effect of Mainstream Swirling on Flowfield Characteristics of an Outer-Cavity Trapped Vortex Combustor

Y. Jin[†], K. Zhang, K. Yao, Y. Wang, D. Wu and X. He

Nanjing University of Aeronautics and Astronautics, Nanjing, Jiangsu, 210016, China

†*Corresponding Author Email: pde_jy@nuaa.edu.cn*

ABSTRACT

Nonreacting flow characteristics are important for determining the performances of combustors. In the present work, the effects of mainstream swirling on the nonreacting flow characteristics of an outer-cavity trapped vortex combustor are investigated by introducing swirlers. The results are first validated by particle image velocimetry measurements by considering four swirl numbers (0, 0.4, 0.6, and 0.8) and three velocity sets. The results show that the addition of swirlers in the mainstream introduces 3D flow not only in the mainstream but also in the cavities. As the swirl number increases, the size of the low-velocity region near the center-line of the combustor increases both in the axial and radial directions. The cavity flow maintains the dual-vortex pattern for most cases; however, for certain cases with high mainstream velocities and high swirl numbers (0.6, 0.8), multiple-vortex patterns are observed. The mixing results are discussed in terms of turbulence intensity and kinetic energy. The turbulence intensities of the combustor outlet for a swirl number of 0.8 are found to increase by approximately 250-350% compared to the case without swirling, indicating dramatically enhanced mixing.

NOMENCLATURE

D	outer diameter of swirler	PS	plane of middle cavity length
d	inner diameter of swirler	RANS	Reynolds-Averaged Navier Stokes
LBO	Lean Blow Out	RNG	Re-Normalization Group
LES	Large Eddy Simulation	s	Thickness of the vanes
L	width of swirl	SST	Shear Stress Transport
n	number of swirl vanes	S_N	swirl number
PIV	Particle Image Velocimetry	TVC	Trapped Vortex Combustor
PM	plane of middle combustor y-direction	β	angle of vanes

1. INTRODUCTION

The trapped vortex combustor (TVC) is a new concept for flame stabilization in aero-engines. For conventional combustor, the recirculation zones are created by swirlers to provide continuous sources of ignition by mixing hot products with fresh air and fuel(see Lefebvre and Ballal (2010)). However, these zones become less stable at higher inlet velocities, leading to inferior combustor performance in terms of flame stability, combustion efficiency and emissions. The TVC is an alternative to the conventional combustor, instead of swirl-stabilization, it utilizes cavities in which vortexes

are trapped to stabilize the flame. Because of the protection of the cavity, the vortex is invulnerable to disturbances from flow conditions, unlike the conventional combustors, thus enabling better flame stability. The TVC was initially proposed by Hsu et al. (2013); Hsu et al. (1999); Hsu et al. (1998), and this configuration has been extensively studied. The US Air Force Research Laboratory (AFRL) has developed four generations of TVCs. The mainstream is dominated by the geometry of the dome, such as the strut, rod, guide vane, and swirler (see Zhao *et al.* (2018)).

Wu *et al.* (2015); Wu *et al.* (2015); Wu *et al.* (2016) focus on the effects of the strut width on

combustion efficiency and emission. The experiment and simulation results show the protection from the wider struts and mixing enhancement from slenderer struts. Li *et al.* (2018); Li *et al.* (2017); Li, He *et al.* (2018) studied the effects of strut length on the ignition, LBO, and combustion efficiency of the TVC by experiments and simulation, results show that the poor ignition performance and LBO limits of the shorter struts are primarily caused by the large amount of mainstream air entrained the cavity; the higher combustion efficiency with the shorter struts is mainly attributed to the wake region formed behind the struts. The combustion characteristics may be mainly attributed to the significant differences in the flow patterns. Jin *et al.* (2014a); Jin *et al.* (2014b); Jin *et al.* (2014c) focus on the effects of the cavity-injector/radial-strut relative positions on the TVC performance. These specific positions include inline, intermediate and staggered arrangement. The good performance of the staggered arrangement is mainly attributed to the counter-rotating streamwise vortex pair, high turbulence kinetic energy, and intensity. Flow fields of the TVC with struts are obtained by particle image velocimetry; it is observed that the radial struts play a key role in the mixing process in the TVC, with the single-vortex pattern behind the struts and dual-vortex pattern between the struts being the two typical cavity vortex flow patterns.

The L-shaped guide vane is proposed by Agarwal *et al.* (2013); Agarwal and Ravikrishna (2011), (2012) as an active strategy to achieve flame stability under all conditions; the guide vane is mounted in the mainstream path to direct a portion of the main flow into the cavity. It could create a desirable dual-vortex in the cavity: a small clockwise vortex behind the vane and large counterclockwise vortex at the bottom of the cavity. The square-tipped and sharp-tipped guide vanes are proposed by Chen and Zhao (2018a), along with numerical investigations of their flowfields and combustion performances. It was observed that the wake vortex instead of cavity bottom vortex becomes the dominant one which contributes to the flame stabilization.

Swirling flow is normal and essential for the conventional gas turbine combustor because it is associated with a large recirculation zone for flame stabilization. Recently, some studies have introduced swirling flow in TVCs. Chen and Zhao (2018b); Song *et al.* (2016) numerically investigated a nonreacting swirling trapped vortex ramjet combustor with two swirler numbers (S_{NS}). The results indicated that significant 3D flow were introduced in the cavity vortex owing to the swirling motions in the combustor; meanwhile, the turbulence intensity and kinetic energy are found to increase by approximately 300%. Further, the effects of strong spinning on the trapped vortex ramjet combustor have been numerically investigated with the inflow boundary set at the rate of 30,000 rpm; the results show that vortex breakdown occurred inside the cavity and the two-vortex structure caused strong 3D flow and promoted fuel-air mixing. Merlin (2013); Merlin *et al.* (2012) proposed an annular TVC burner, where a pilot flame in the cavity generated burnt gases that are drained into the mainstream by the suction generated by the rods mounted in the mainstream; it should be noted here that a swirler with S_N=1.52 is mounted on the upstream of the rod. Adding swirl allows more efficient mixing, with two strong main vortices and sufficient fluid exchange between the cavity and main flow.

The distinction between combustion performance under flat, jet, or swirling flow is considerably different. Recent research indicates that airflow in the cavity region has some characteristics of centrifugal forces and circular motion under swirling flow, which introduces some essential changes to the combustion. Katta *et al.* (2013); Lewis (1971); Lewis *et al.* (1977).

It can be seen from the above discussion that mainstream flow mixing remains a critical issue in the TVC, and very strong interactions exist between the mainstream and cavity flow. In the present work, the introduction of swirling flow in the mainstream using axial swirlers to enhance mainstream mixing is examined. The focus of this work is not only on the quantitative evaluation of mainstream mixing enhancement but also on the interaction of the swirling flow, featuring centrifugal forces and circumferential motions, with the complex cavity flow.

2. MODELS AND RESEARCH METHODS

2.1 Configuration of Combustor Model

The combustor is a can-shaped device with an external cavity, with the mainstream channel located inside, as shown in Fig. 1. The depth and length of the cavity are 43 mm and 50 mm, respectively. The distance from the center of the cavity fore wall slot to the bottom wall is 6 mm, while that from the cavity after wall slot is 20 mm. The width of each both slot is 4mm. The flow is specified as the x-direction, and the radial direction of the model is the y-direction.
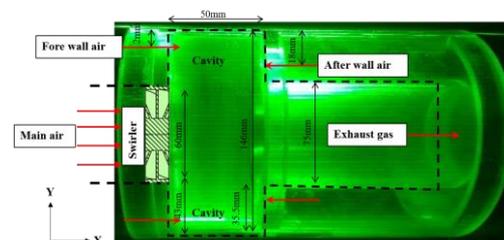

Fig. 1. Scheme of the combustor model.

A single axial swirler is set at the main flow outlet, and its schematic is as shown in Fig. 2. Additionally, straight vanes are used. The main geometrical parameters of the axial swirler are as follows: inner diameter d and outer diameter D; installation angle β of the vanes; number of vanes n; thickness of the vanes s. In view of the

experimental assembly, the outer diameter of the swirler is set as a constant 56 mm, and the thickness of the vane is 1mm. The swirler number is obtained using Eq. (1):

$$S_N = \frac{2}{3}\left[\frac{1-\left(d/D\right)^3}{1-\left(d/D\right)^2}\right]\tan\beta \qquad (1)$$

The geometrical information of the four swirlers is given in Table 1. It should be noted that the no swirler condition is considered as the baseline case.
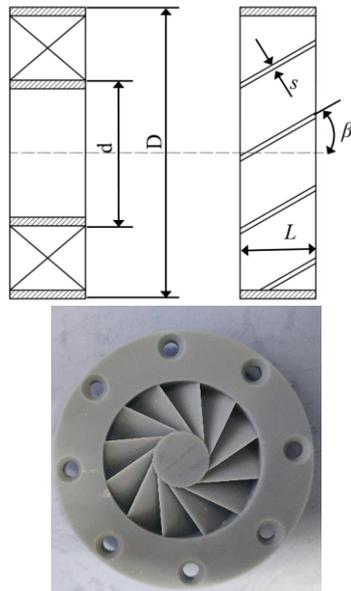

Fig. 2. Scheme of the axial swirler.

Table 1 Swirler geometry.

| Number	1	2	3	4
D (mm)	56	56	56	56
d (mm)	20	20	20	20
L (mm)	15	15	15	15
β (°)	0	30	40	50
n	16	16	12	12
s	1	1	1	1
S_N	0	0.4	0.6	0.8

2.2 Experimental Setup

As a noncontact flow-field measurement method, particle image velocimetry (PIV) method has advantages such as no effect on the original flow-field and accurate measurement. The PIV system produced by La Vision mainly includes two parts: laser generator and data acquisition system. Two continuous-wave pumped Q-switched Nd:YLF DPSS laser resonators were used, and the maximum power and wavelength were 200 MJ and 527 nm, respectively. The time interval between pulses is 0.50 μs to 33.3 ms. The charge coupled device (CCD) camera has a spatial resolution of 1280×800 pixels with the maximum frame rate of 7400 fps. The exposure time of the CCD camera and illumination time of the laser were controlled with a time board integrated with the PC. Instantaneous velocity vector fields were generated by a cross-correlation technique between successive particle images.

The experimental system is shown in Fig. 3 and designed according to the combustion chamber model and PIV system requirements, which mainly comprise three parts, namely the air supply system, particle seeding facilities, and PIV system. The cavity airflow is supplied by the air source I, and the maximum flow is 30 m³/h. A bypass valve is set on the upstream branch to discharge the flow. The airflow entering the cavity fore wall and after wall slots are controlled using mass flow controllers. The flow range of the mass flow controller is 0 to 60 m³/h, its accuracy is ± 2%, and the repetition accuracy is ± 0.2%. The direction of airflow is shown by the arrow in the figure. Air source II is provided by the root blower, and its maximum flow is 3400 m³/h. The vortex flowmeter used is the DN50, whose measurement range is 35 to 380 m³/h, and its accuracy is ± 1.5%.

2.3 Numerical Simulation

2.3.1 Mesh Generation

To ensure that the calculated results are independent of the grid, a grid sensitivity study is conducted,
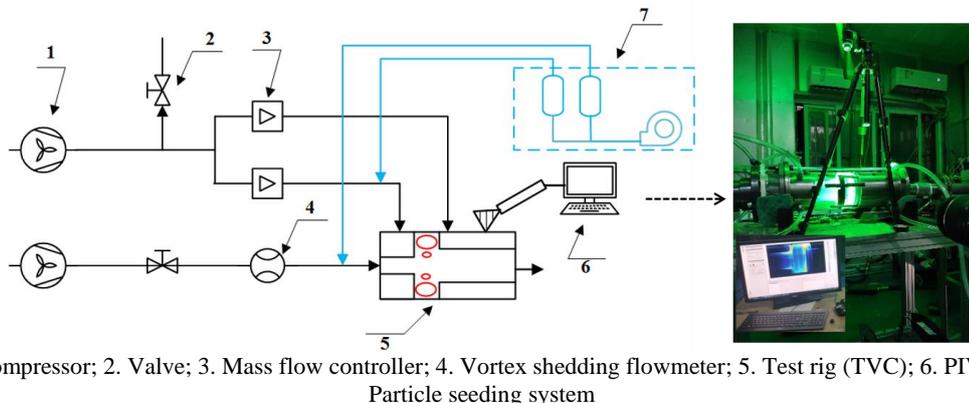
1. Compressor; 2. Valve; 3. Mass flow controller; 4. Vortex shedding flowmeter; 5. Test rig (TVC); 6. PIV; 7. Particle seeding system

Fig. 3. Schematic of the experimental setup.

as shown in Fig. 4 The results of grids G1, G2, G3 and G4 are compared in terms of the mean x velocity profiles at x/L=0.3, 0.5, and 0.7 (where x represents the axial distance and L represents the axial length of the cavity) in the x-y plane. The maximal mean x velocity deviation between G2 and G3 is approximately 25%, and the deviation between G3 and G4 is about 4%. Therefore, G3 is adopted in the present work. The number of cells for each grid is listed in Table 2.

Table 2 Details of the four grids used in the grid independency study.

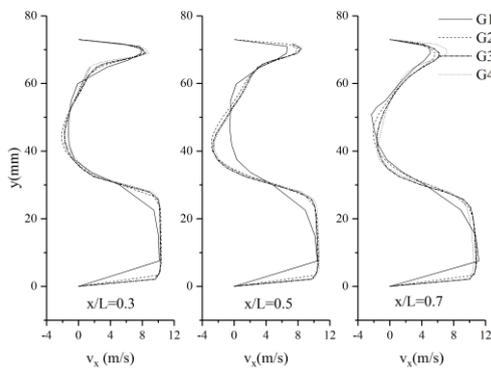|	G1	G2	G3	G4
Number of cells	502345	712367	1659836	2010012

Fig. 4. Radial profiles of mean x velocity at x/L=0.3, 0.5, and 0.7 for S_N=0, case2.

2.3.2 Boundary Conditions

The mass flow inlet is used for all inflow boundaries and pressure outlet for the exit; the static pressure and temperature are maintained as 101325 Pa and 300 K, respectively. Additionally, no-slide walls are applied for the other faces of the model, standard wall treatment in the CFD code is applied. The incompressible ideal gas is adapted to the present simulation, and the SIMPLE algorithm is employed for pressure-velocity coupling. The second-order upwind scheme is invoked for the convection and diffusion terms. The present numerical work are implemented in ANSYS Fluent. The mass flow rate for each inlet is listed in Table 3, where case1 is regarded as the baseline case. Momentum at different inlet conditions is shown in Fig. 5.

Table 3 Test conditions for swirling TVCs.

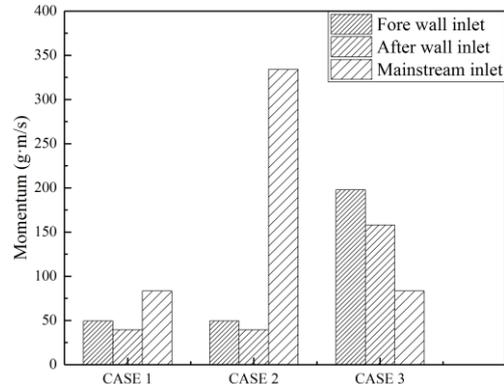|	Parameter	Fore wall inlet	After wall inlet	Mainstream
Case 1	Flow(g/s)	9.9	7.9	16.7
	V(m/s)	5	5	5
Case 2	Flow(g/s)	9.9	7.9	33.4
	V(m/s)	5	5	10
Case 3	Flow(g/s)	19.8	15.8	16.7
	V(m/s)	10	10	5

Fig. 5. Momentum at inlet.

A series of simulations was conducted to explore the cold flow of the annular TVC with the swirler mounted in the mainstream. The results for velocity, turbulence intensity, and vortex dynamics were discussed in detail. Two planes of interest in simulation, designated as PM (plane of middle combustor y-direction), PS (plane of middle cavity length) is shown as Fig. 6.
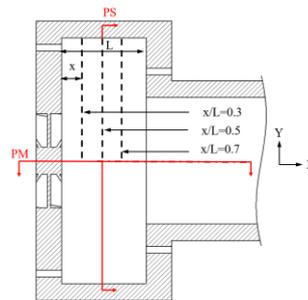

Fig. 6. Two planes and three lines, designated as PM, PS, x/L=0.3, x/L=0.5, and x/L=0.7.

2.3.3 Turbulence Model Determination and Numerical Method Validation

The two-equation Standard k-ε turbulence model was adopted by Li, He, Zhao, Jin, Ge, *et al.* (2018a); Li *et al.* (2017); Li, He, Zhao, Jin, Yao, *et al.* (2018b) for the TVC simulation. Additionally, the two-equation model Shear Stress Transport (SST) k-ω turbulence model was used by Agarwal *et al.* (2013); Agarwal and Ravikrishna (2011), (2012). The Reynolds Stress Model was used for 3D numerical investigations of swirling trapped vortex ramjet combustor. Chen and Zhao (2018b). In the present work, Standard k-ε model, Re-Normalization group (RNG) k-ε, Realizable k-ε and Standard k-ω models are compared with the PIV results. The mean x velocity profiles at x/L=0.3, 0.5, and 0.7 in the x-y plane are represented in Fig. 7. The velocity of the wall region can not be represented adequately in the PIV measurements. It should be noted that all four turbulence models can capture the mean axial velocity distributions; however, the mean axial velocity deviation between the Realizable k-ε turbulence model result and the
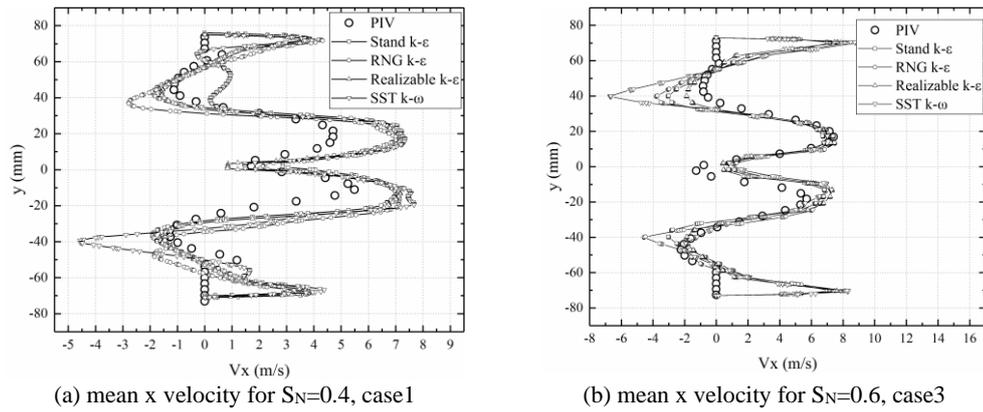
(a) mean x velocity for S_N=0.4, case1   (b) mean x velocity for S_N=0.6, case3

Fig. 7. Radial profiles of mean x velocity at x/L=0.3 for several turbulent models.
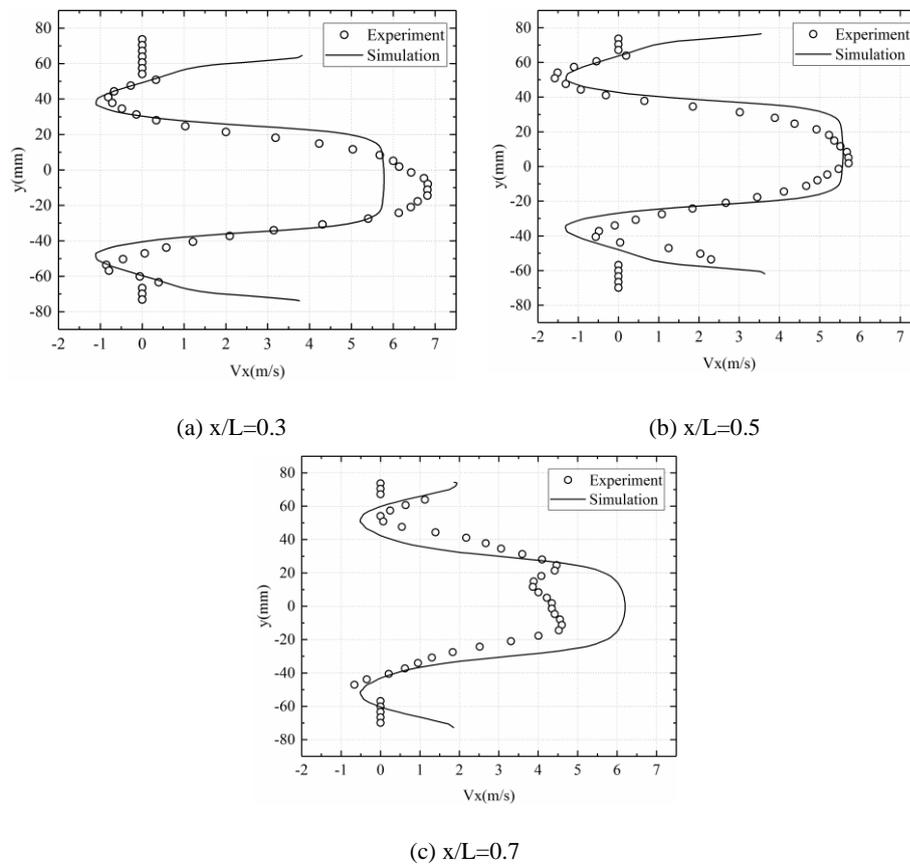

(a) x/L=0.3   (b) x/L=0.5

(c) x/L=0.7

Fig. 8. Radial profiles of mean x velocity at x/L=0.3, 0.5, and 0.7 for S_N=0, case1.

PIV result are minimum. Therefore, the Realizable *k-ε* turbulence model is able to satisfactorily predict the current combustor flowfields in swirling flow. Meanwhile, the mean x velocities at x/L=0.3, 0.5, and 0.7, as computed by the Realizable *k-ε* model, are compared with the experimental results, as shown in Fig. 8 and Fig. 9 for S_N=0 and S_N=0.6 with different case. It is evident that the predicted results reproduce the cavity flow features qualitatively. In the cavity, the predicted velocity agrees well with the experimental results, although the axial velocities in the mainstream and the near-wall region show discrepancies.

3. RESULTS AND DISCUSSION

3.1 Effect of Swirl Number on Combustor Flow Pattern

In general, the axial, radial and tangential velocities are used to describe airflow with rotating motion. Intense interactions between the mainstream and cavity flow can be expected along the boundary between these two areas, and the interactions are examined at turbulence levels. Figure 10 shows the streamlines overlaid on the contours of the velocity
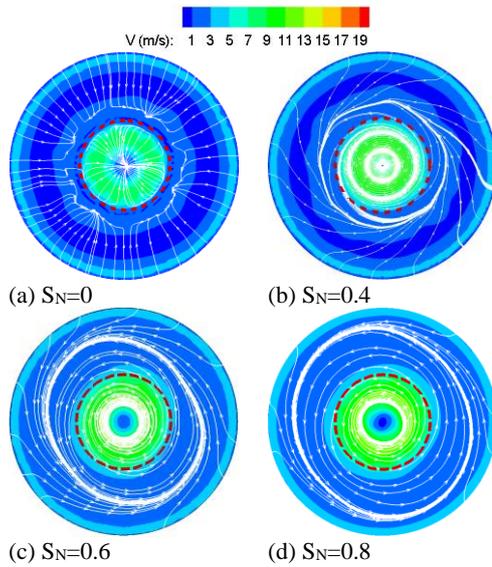
(a) x/L=0.3

(b) x/L=0.5

(b) x/L=0.7

Fig. 9. Radial profiles of mean x velocity at x/L=0.3, 0.5, and 0.7 for S_N=0.6, case2.

magnitude in the PM plane for case1; the velocity of cavity fore wall jet, after wall jet, and mainstream are all 5m/s; four swirl numbers are considered. In the mainstream region, the flow patterns show obvious variations as S_N changes. For S_N=0, a low-velocity recirculation zone is formed near the center-line of the combustor, and the length of this recirculation zone is about 50 mm. As the swirl number increases, the size of this low-velocity zone increases both in the axial and radial directions, indicating enhanced swirling motion, which is believed to be helpful for mixing. In the cavities, the flow maintain typical dual-vortex patterns, where a primary vortex is locked deeply in the cavity and a second small vortex is locked between the primary vortex and mainstream. The variation of S_N in the mainstream shows little influence on the cavity flow pattern.

Figure 11 depicts the streamlines overlaid on the contours of the velocity magnitude in the PS plane for case1, and the red dashed circles denote the boundary regions between the cavity and mainstream. The tangential velocity profiles along the radial direction at x/L = 0.3, 0.5, and 0.7 in the PM are shown in Fig. 12. From both figures, the effects of the swirl number on rotating motion are immediately apparent. No rotating flow is observed at S_N=0; as the S_N increases, the tangential velocity increases both in cavity and mainstream. For instance, the tangential velocities at the points (x/L =0.5、y=30 mm, in the cavity) corresponding to S_N of 0.4, 0.6, and 0.8 are 2.2m/s, 4m/s, and

(a) S_N=0 (b) S_N=0.4

(c) S_N=0.6 (d) S_N=0.8

Fig. 10. Streamlines overlaid on the contours of velocity magnitude, PM, case1.

6m/s, respectively; the tangential velocities at the points (x/L=0.5, y=15 mm, in the mainstream) corresponding to S_N of 0.4, 0.6, and 0.8 are 6 m/s, 8.2 m/s, and 10 m/s, respectively.

(a) $S_N=0$ (b) $S_N=0.4$

(c) $S_N=0.6$ (d) $S_N=0.8$

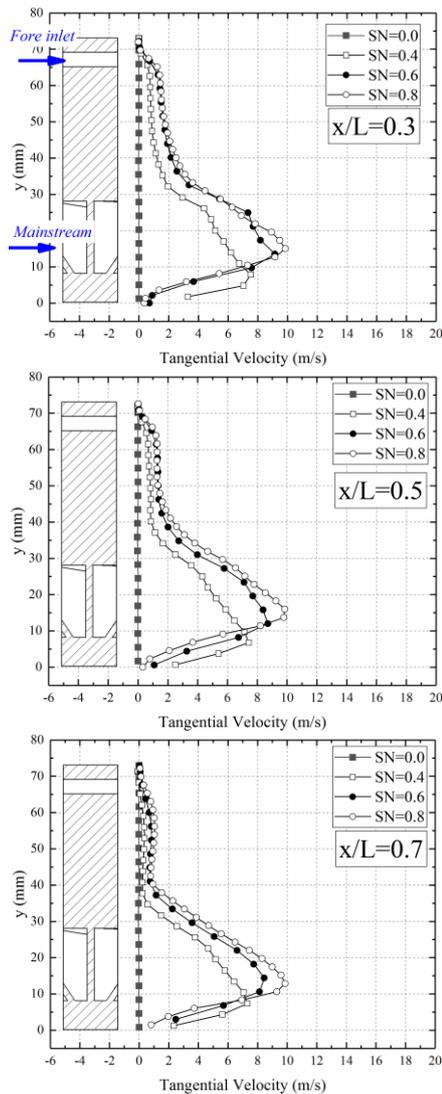**Fig. 11. Streamlines overlaid on the contours of velocity magnitude, PS, case1.**

Fig. 12. Radial profiles of mean tangential velocity, case1.

Figure 13 depicts the streamlines overlaid on the contours of velocity magnitudes in the PM plane for case2; the velocities of the cavity fore wall and after wall jets are 5m/s, as in case1, and the mainstream velocity is 10m/s, which is twice that in case1. The flow pattern in the mainstream is similar to that in case1, although the overall sizes of the low-velocity recirculation zones are larger compared with those of case 1 owing to the increased mainstream velocity. In the cavities, however, interestingly, the flow patterns vary with S_N increases significantly. For $S_N=0$, the cavity flow features the typical dual-vortex pattern mentioned above. As S_N increases to 0.4, the secondary vortexes disappear, sizes of the primary vortexes decrease, and vortex cores of the primary vortexes shift toward the upstream slightly. For $S_N=0.6$, the cavity features a multiple-vortex pattern. The size of the primary vortex is reduced to 50% that of case 1, and this vortex further shifts upstream. A very small vortex is observed in the cavity upstream corner, and a big vortex is formed in the cavity downstream corner. As the S_N increases to 0.8, the cavity retains the multiple-vortex flow feature; however, the primary vortex moves further upstream and the two corner vortexes are of the same size.
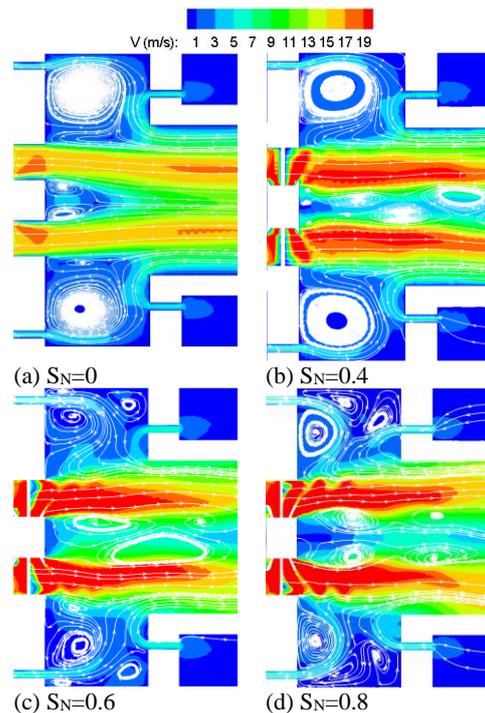

(a) $S_N=0$ (b) $S_N=0.4$

(c) $S_N=0.6$ (d) $S_N=0.8$

Fig. 13. Streamlines overlaid on the contours of velocity magnitude, PM, case2.

The two cavity corner vortexes and their behaviors evidence that the penetration depth of the cavity fore wall jet decreases as the mainstream swirl number increases. This phenomenon can be explained thus: the cavity fore wall jet direction is more dependent on the mainstream in case2 than case1, as the mainstream momentum in case2 is four times that of case1. As the mainstream S_N

increases, the direction of the cavity fore wall jet changes earlier, which leads to reduced penetration depth of the cavity fore wall jet. Figure 14 shows the streamlines overlaid on the contours of the tangential velocity magnitudes in the PS plane for case 2. Figure 15 shows the tangential velocity profiles along the radial direction at x/L = 0.3, 0.5, and 0.7 in the PM, quantitatively showing that tangential velocity increases with the S_N increases.
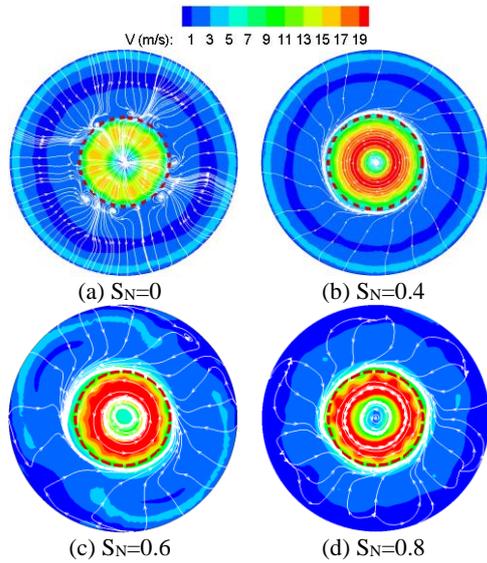

(a) S_N=0   (b) S_N=0.4

(c) S_N=0.6   (d) S_N=0.8

Fig. 14. Streamlines overlaid on the contours of velocity magnitude, PS, case2.

Figure 16 shows the streamlines overlaid on the contours of the velocity magnitudes in the PM plane for case3; the velocities of the cavity fore wall and after wall jets are both 10m/s, which is twice that of case1, and the mainstream velocity is 5 m/s, which is the same as that of case1. It is noteworthy that the flow pattern in the mainstream is quite different from that of case1 or case2, and the low-velocity regions are very small in size for the four swirl numbers, which is beyond prediction. However, the cavity flow pattern is similar to that of case1, and the dual-vortex pattern is slightly changed as the swirl number varies. The reason for this is that as the velocities of the cavity fore wall and after wall jets increase to 10 m/s, the momentum of cavity flow increases by four times as compared to case1, so cavity flow plays a dominant role in determining the combustor flow pattern. The higher the cavity flow momentum, the more confinement effect would be encountered with the mainstream swirling flow; therefore, the low-velocity regions become smaller compared with those of case1 and case 2.

Streamlines plotted in the PS plane for four swirl numbers are shown in Fig. 17. It can be seen that there are dense-streamline featured boundaries which separate the flow region into two parts. The boundaries are believed to be the shear layers between the mainstream and cavity flow. The region inside the boundaries are mainstream, while the region outside the boundaries are cavity flow.
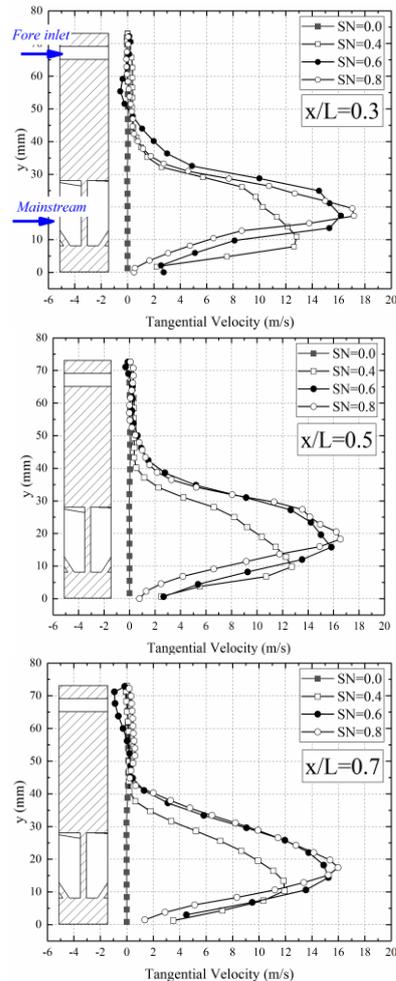

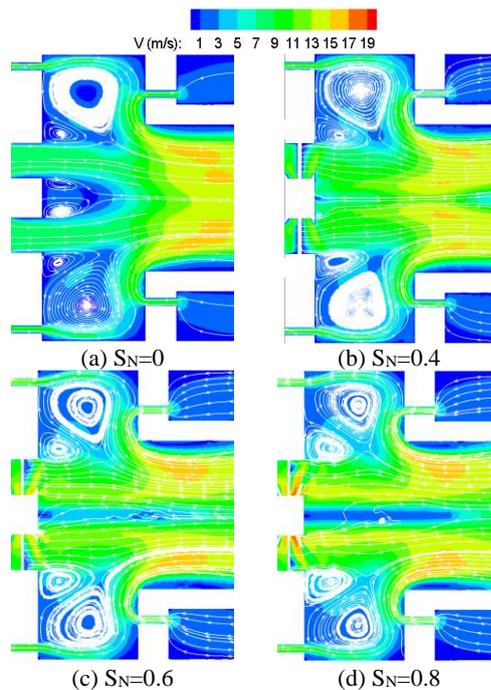**Fig. 15. Radial profiles of mean tangential velocity, case2.**

(a) S_N=0   (b) S_N=0.4

(c) S_N=0.6   (d) S_N=0.8

Fig. 16. Streamlines overlaid on the contours of velocity magnitude, PM, case3.
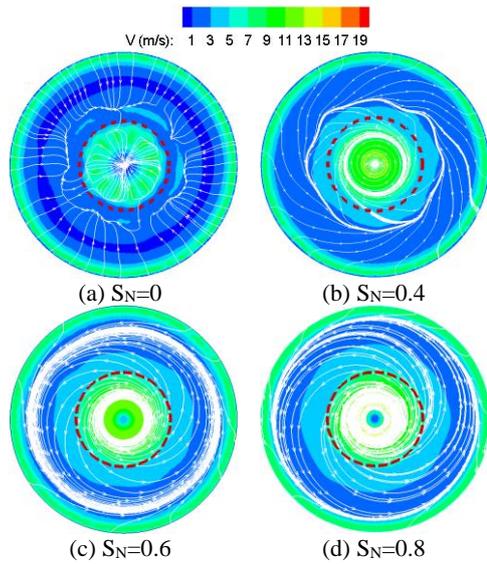
Fig. 17. Streamlines overlaid on the contours of velocity magnitude, PS, case3.
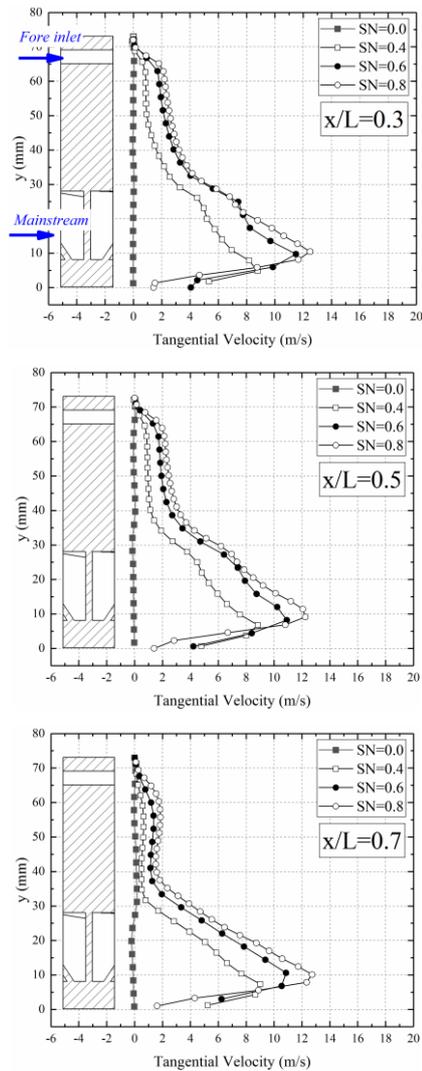

Fig. 18. Radial profiles of mean tangential velocity, case3.

All three cases share some similarities where the boundaries shift outwards in the radial direction as the swirl number increases, indicating that more regions are affected by mainstream swirling flow as the swirl number increases. Figure 18 shows the tangential velocity profiles along the radial direction at x/L = 0.3, 0.5, and 0.7 in the PM, quantitatively showing that tangential velocity increases with the S_N increases.

3.2 Effect of Swirl Number on Turbulence intensity and kinetic energy

In combustor applications, turbulence activities play a crucial role in mixing and combustion. Turbulence is characterized by velocity fluctuations; fuel-air mixing and combustion can be significantly enhanced in the high turbulence region. It is meaningful to evaluate the turbulence levels in nonreacting flow in the TVC with mainstream swirling addition, although chemical reactions are not considered in this work.

Distributions of the turbulence intensity are termed case1, case2, and case3 and provided in Fig. 19, Fig. 20, Fig. 21, respectively. It can be seen that the large turbulence intensity regions are mainly located at the mainstream-cavity shear layers, and the shear layers develop with increasing sizes as flow downstream. As the swirl number increases, the turbulence intensity increases significantly, both in the cavity and in the mainstream. For case 1, the turbulence intensity in the shear layer increases from 10% to 30% as swirl number increases from 0 to 0.8, and the average turbulence intensity in the outlet increases from 10% to 30%. These results are encouraging as the mixing and combustion in the mainstream may be greatly enhanced by the addition of swirling.
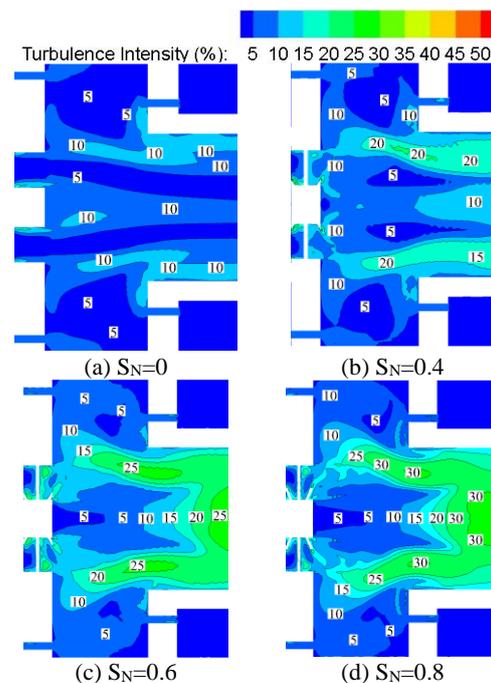

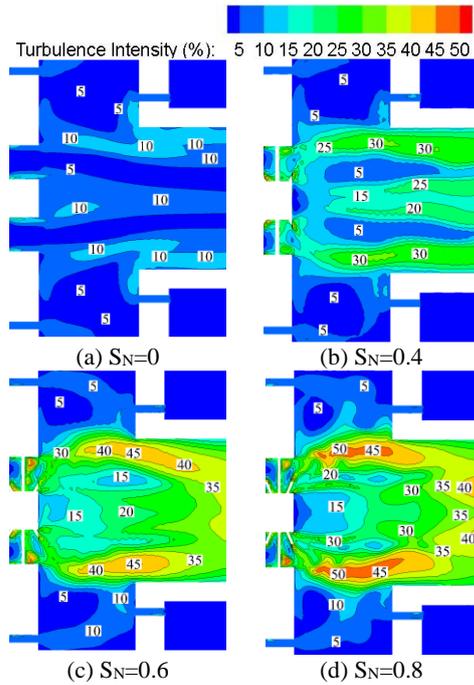**Fig. 19. Turbulence intensity distributions, PM, case1.**

(a) $S_N=0$ (b) $S_N=0.4$

(c) $S_N=0.6$ (d) $S_N=0.8$

Fig. 20. Turbulence intensity distributions, PM, case2.

(a) $S_N=0$ (b) $S_N=0.4$

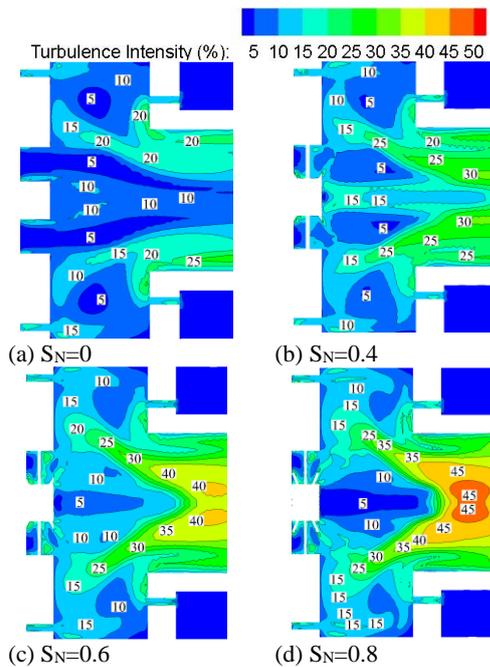(c) $S_N=0.6$ (d) $S_N=0.8$

Fig. 21. Turbulence intensity distributions, PM, case3.

The average turbulence intensity in the cavity with different S_N under three cases are shown in Fig. 22. When there is no swirling flow, i.e., $S_N=0$, the turbulent intensity is mainly affected by the mass flow rate and is about 5% for case1 and case2, and about 10% for case3. The turbulent intensity increases with increase of the S_N for all cases; when S_N increases to 0.8, the turbulent intensity increases to 9%, 11%, and 13%. The maximum value of turbulence intensity for case 3 thus increases by
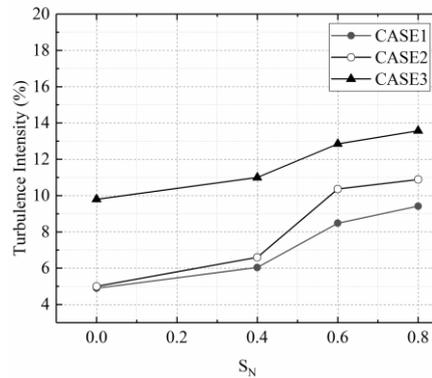
approximately 30% compared with that of case 1.

Fig. 22. Averaged turbulence intensity in the cavity zone.

Figure 23 shows the turbulence kinetic energy iso-surface for $S_N=0$ and $S_N=0.6$ under case 2. Similar results for increase in the turbulence kinetic energy can be seen as the S_N increases. The high turbulence kinetic energy regions are also located in the shear layer between the mainstream and cavity.
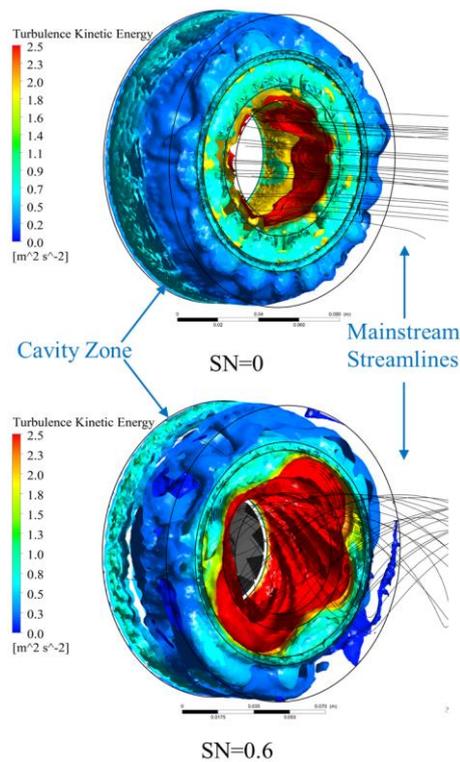

Fig. 23. Turbulence kinetic energy iso-surfaces for case2.

3.3 Cavity Vortex Dynamics

The schematic in Fig. 24 is an attempt to illustrate the main flow features identified by the numerical simulations in the present study. For conventional TVCs, the dual vortex is locked in the cavity produced by the three air jets, and the mixing of the different primary vortexes is low. The mainstream in the TVC flow has the characteristics of a parallel

straight flow. When the TVC is operated with the addition of swirling in the mainstream, the significant alteration in the mainstream is the velocity direction, which features obvious radial and tangential velocity. The tangential velocity of the cavity flow is therefore attained with the drag of the swirling mainstream flow. Cavity air in the cavity region acts as a spring spiral flow, as shown in Fig. 24. This unique flow pattern can be regarded as the combined result of two typical motions: one is the dual vortex driven by the cavity air and mainstream, and the other is the rotation around the axis caused by the swirling mainstream.

It can be inferred from the flow patterns that the mixing in both the mainstream and cavity can be enhanced, and the interactions between the mainstream and cavity flow can also be enhanced. Therefore, the TVC with mainstream swirling is an alternative and promising, robust and efficient combustor concept.
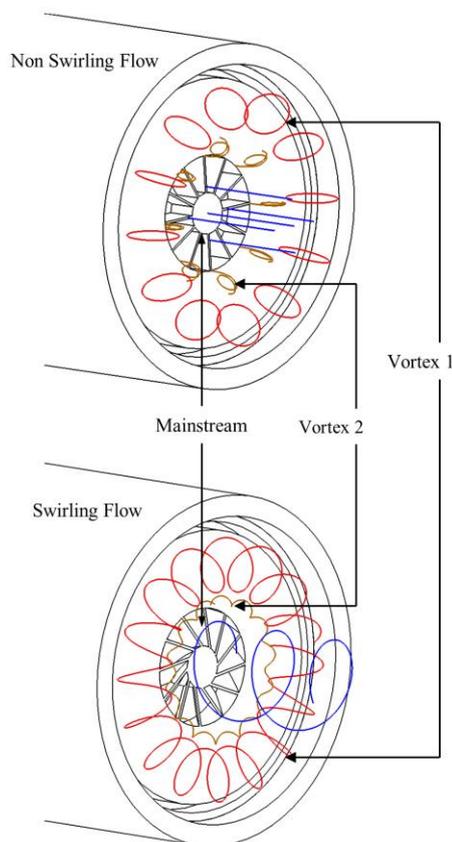

Fig. 24. Schematic of the vortex structures in the TVC and TVC with swirler.

4. CONCLUSION

In this work, mixing enhancement in the TVC is proposed using swirlers in the mainstream, and 3D numerical investigations are performed to verify this. The numerical methods are first validated with PIV experiment results. Twelve cases are computed with four swirl numbers (0, 0.4, 0.6, and 0.8) and three velocity sets. The results show that the

addition of swirlers in the mainstream introduces 3D flow not only in the mainstream but also in the cavities. Besides, the swirl number and velocity sets both influence the nonreacting flow characteristics of the combustor.

As the swirl number increases, the size of the low-velocity region near the combustor center-line increases both in the axial direction and radial directions. The cavity flow maintains the dual-vortex pattern for most cases; however, for certain cases with high mainstream velocity and high swirl number (0.6, 0.8), multiple-vortex patterns are observed. This is significant as the cavity flow pattern is a decisive factor associated with flame stability.

The mixing results are discussed in terms of turbulence intensity and kinetic energy. The turbulence intensities of the combustor outlet for swirl number 0.8 are found to increase significantly by approximately 250-350% compared to the case without swirling, which indicates the dramatically enhanced mixing.

What remains to be investigated in future work is the combustion experiments of this outer-cavity trapped vortex combustor with mainstream swirling, with focus on the flame stability and combustion efficiency, both of which could further validate the results of the present work.

REFERENCES

Agarwal, K. K., S. Krishna and R. V. Ravikrishna (2013). Mixing Enhancement in a Compact Trapped Vortex Combustor. *Combustion Science and Technology* 185, 363-378.

Agarwal, K. K. and R. V. Ravikrishna (2011). Experimental and Numerical Studies in a Compact Trapped Vortex Combustor: Stability Assessment and Augmentation. *Combustion Science and Technology* 183, 1308-1327.

Agarwal, K. K. and R. V. Ravikrishna (2012). Validation of a Modified Eddy Dissipation Concept Model for Stationary and Nonstationary Turbulent Diffusion Flames. *Combustion Science and Technology* 184, 151-164.

Chen, S. and D. Zhao (2018a). Numerical study of guide vane effects on reacting flow characteristics in a trapped vortex combustor. *Combustion Science and Technology* 190, 2111-2133.

Chen, S. and D. Zhao (2018b). Numerical study of non-reacting flowfields of a swirling trapped vortex ramjet combustor. *Aerospace Science and Technology* 74, 81-92.

Hsu, K., C. Carter, V. Katta and W. Roquemore, (1999). Characteristics of combustion instability associated with trapped-vortex burner. In *37th Aerospace Sciences Meeting and Exhibit*.

Hsu, K., L. Gross, D. D. Trump and W. M. Roquemore (2013). Performance of a trapped-vortex combustor. In *Aerospace Sciences Meeting & Exhibit*.

Hsu, K. Y., L. P. Goss and W. M. Roquemore (1998). Characteristics of a trapped-vortex (TV) combustor. *Journal of Propulsion Power* 14, 57-65.

Jin, Y., X. He, B. Jiang, Z. Wu, G. Ding and Z. Zhu (2014a). Effect of cavity-injector/radial-strut relative position on performance of a trapped vortex combustor. *Aerospace Science and Technology* 32, 10-18.

Jin, Y., X. He, J. Zhang, B. Jiang and Z. Wu (2014b). Numerical investigation on flow structures of a laboratory-scale trapped vortex combustor. *Applied Thermal Engineering* 66, 318-327.

Jin, Y., Y. Li, X. He, J. Zhang, B. Jiang, Z. Wu and Y. Song (2014c). Experimental investigations on flow field and combustion characteristics of a model trapped vortex combustor. *Applied Energy* 134, 257-269.

Katta, V., D. Blunck and M. Roquemore (2013). Effect of Centrifugal Forces on Flame Stability in an Ultra-Compact Combustor. In *Aiaa Aerospace Sciences Meeting Including the New Horizons Forum & Aerospace Exposition*.

Lefebvre, A. H. and D. R. Ballal (2010). *Gas Turbine Combustion - 3rd Edition*. New York: Taylor&Francis Group.

Lewis, G. D. (1971). Combustion in a centrifugal-force field. *Symposium (International) on Combustion* 13, 625-629.

Lewis, G. D., J. H. Shadowen and E. B. Thayer (1977). Swirling Flow Combustion. *Journal of Energy* 1(4), 201-205.

Li, M., X. He, Y. Zhao, Y. Jin, Z. Ge and W. Huang (2018a). Effect of strut length on combustion performance of a trapped vortex combustor. *Aerospace Science and Technology* 76, 204-216.

Li, M., X. He, Y. Zhao, Y. Jin, Z. Ge and Y. Sun (2017). Dome structure effects on combustion performance of a trapped vortex combustor. *Applied Energy* 208, 72-82.

Li, M., X. He, Y. Zhao, Y. Jin, K. Yao and Z. Ge (2018b). Performance enhancement of a trapped-vortex combustor for gas turbine engines using a novel hybrid-atomizer. *Applied Energy* 216, 286-295.

Merlin, C. (2013). *Simulation numérique de la combustion turbulente : Méthode de frontières immergées pour les écoulements compressibles, application à la combustion en aval d'une cavité.*

Merlin, C., P. Domingo and L.Vervisch (2012). Large Eddy Simulation of turbulent flames in a Trapped Vortex Combustor (TVC) – A flamelet presumed-pdf closure preserving laminar flame speed. *Comptes Rendus Mécanique* 340, 917-932.

Song, C., R. Chue, S. Yu and J. U. Schluter (2016). Spinning Effects on a Trapped Vortex Combustor. *Journal of Propulsion Power* 32(5), 1-13.

Wu, Z., X. He, B. Jiang and Y. Jin (2015). Experimental investigation on a single-cavity trapped vortex combustor. *International Communications in Heat and Mass Transfer* 68, 8-13.

Wu, Z., X. He, Y. Jin, Y. Song and Y. Zhu (2016). Impact of interaction between cavity flow and mainstream on the performance of a model trapped vortex combustor. *Journal of Aerospace Engineering* 230, 1181-1200.

Wu, Z., Y. Jin, X. He, C. Xue and L. Hong (2015). Experimental and numerical studies on a trapped vortex combustor with different struts width. *Applied Thermal Engineering* 91, 91-104.

Zhao, D., E. Gutmark and P. de Goey (2018). A review of cavity-based trapped vortex, ultra-compact, high-g, inter-turbine combustors. *Progress in Energy and Combustion Science* 66, 42-82.